*Clays and Clay Minerals*, Vol. 45, No. 1, 54–67, 1997.

# TRANSFORMATION OF SMECTITE TO ILLITE IN BENTONITE AND ASSOCIATED SEDIMENTS FROM KAKA POINT, NEW ZEALAND: CONTRAST IN RATE AND MECHANISM

GEJING LI,[1]† DONALD R. PEACOR[1] AND DOUGLAS S. COOMBS[2]

[1]Department of Geological Sciences, University of Michigan, Ann Arbor, Michigan 48109-1063

[2]Geology Department, University of Otago, Dunedin, New Zealand

**Abstract**—Smectite and mixed-layer illite/smectite (I/S) in Triassic heulandite-rich bentonite from Kaka Point, New Zealand, have been investigated by scanning electron microscopy (SEM), transmission electron microscopy/analytical electron microscopy (TEM/AEM) and X-ray diffraction (XRD) for comparison with matrix phyllosilicates in closely associated siltstones and analcimized tuff. Samples that were treated to achieve permanent expansion showed that some smectite in bentonite occurs as curved packets of wavy 10.5- to 13-Å layers enveloping relict glass shards, the centers of which consist of an amorphous clay precursor. The dominant clay minerals in bentonite are smectite-rich randomly disordered (R0) I/S with variable proportions of 10-Å illite-like interlayers, only locally organized as 1:1 ordered (R1) I/S. R0 I/S was also observed in separate packets retaining the detailed texture of packets that replaced shards. Such relations are consistent with a "solid-state"-like, layer-by-layer replacement of original smectite layers by illite-like layers with partial preservation of the primary smectite texture, in contrast to textures observed elsewhere, such as in Gulf Coast mudstones. The smectite, as in other examples in marine sediments, has K as the dominant interlayer cation, suggesting that precursor smectite may be a major K source for reaction to form illite.

Only a small proportion of illite (35%) occurs in mixed-layer smectite-rich I/S in bentonite and the dominant trioctahedral phyllosilicate is disordered high-Fe berthierine, implying that little mineralogical change has occurred with burial. This contrasts with observations of closely associated siltstones and analcimized tuff, which contain well-defined packets of illite and chlorite but which have no detectable matrix smectite component. These data imply that the rate of transformation of smectite to illite is much slower in bentonites than in associated sediments of the same burial depth and age. Such relations emphasize the significance of factors other than temperature, (e.g., organic acids, permeability and pore fluid compositions) in affecting the rate and degree (and perhaps mechanism) of transformation of smectite to illite.

**Key Words**—Analcimized Tuff, Bentonite, Berthierine, Illite, Kaka Point, Mixed-layer I/S, New Zealand, Siltstone, Smectite, Zeolite Facies.

## INTRODUCTION

As a fundamental process that occurs during diagenesis of argillaceous sediments, the smectite-to-illite transition has been studied extensively for more than 3 decades (Powers 1959, 1967; Burst 1969; Hower et al. 1976; Boles and Franks 1979; Nadeau et al. 1985; Yau et al. 1987; Ahn and Peacor 1986, 1989; Freed and Peacor 1989; Inoue et al. 1990; Buatier et al. 1992). These studies suggest a trend of an increasing proportion of illite within mixed-layer illite/smectite (I/S) with increasing depth or temperature, a relation which has been used as an empirical geothermometer (Perry and Hower 1970, 1972; Hoffman and Hower 1979; Pytte and Reynolds 1989; Pollastro 1989, 1990, 1993; Price and McDowell 1993).

However, the extent of the smectite-to-illite transition is not just a simple function of depth (or temperature), as the phases are metastable and their occurrences are therefore controlled by factors that influence reaction rates, only one of which is temperature (Essene and Peacor 1995). This is demonstrated in part by comparing the evolution of mixed-layer I/S with the maximum temperatures experienced by sediments in various sedimentary basins (Lahann 1980; Środoń and Eberl 1984; Velde et al. 1986; Freed and Peacor 1989). One key aspect of the significance of kinetic (non-equilibrium) factors is in the coexistence of complex heterogeneous I/S materials (e.g., randomly interstratified and ordered I/S). Similarly, the transformation has apparently evolved to different degrees in different rock types at the same burial depth. This has been demonstrated by Masuda et al. (1996), who studied the evolution of I/S in bentonites and shales obtained from a core from Ocean Drilling Program (ODP) site 808 in the Nankai Trough. They showed that mixed-layer I/S is dominant at an early stage of diagenesis in shales, whereas smectite occurs in bentonites with no trace of illite to the greatest depths sampled. Tribble and Wilkens (1994) reported similar relationships between interbedded ash beds and background sediments in ODP site 808, Nankai Trough.

† Current address Department of Geology, Arizona State University, Box 871404, Tempe, Arizona 85287-1404.

Using SEM and TEM, Ahn et al. (1988) observed interlayering of illite in "chlorite" crystals, but no interlayered chlorite, smectite or other phyllosilicates in illite crystals in an analcimized tuff from near Kaka Point in southern New Zealand. The locality is within the general region of the type occurrence of the zeolite facies. A bentonite at nearly the same depth in the sediment column was shown by XRD to have smectite as the dominant clay mineral. This relation is somewhat similar to the observation by Masuda et al. (1996) that transformation of smectite to illite occurs more slowly in bentonitic sediments than in shales of the same burial depth and age. However, no systematic TEM observations were made on the bentonites of Ahn et al. (1988). The detailed structural, textural and chemical relations of clay minerals and their relations to other phases remained undefined. More importantly, the authigenic clay minerals in the closely associated and dominant surrounding siltstones remained poorly characterized. The factors influencing the transformation mechanism of smectite to illite in the bentonite, by comparison with those in analcimized tuff and siltstones, were not investigated.

In this study, we have therefore used XRD, SEM and TEM/AEM to characterize the microstructure, chemical composition and textural relationship of clay minerals in bentonite from Kaka Point, New Zealand. In order to compare the I/S transition in bentonite with those in interbedded analcimized tuff and siltstones that were buried to essentially the same depth as the bentonite, we have characterized the authigenic clay minerals in selected siltstones. These rocks are petrographically similar to rocks described from the Taringatura and Hokonui Hills in the Southland Syncline to the northwest of Kaka Point (Boles and Coombs 1975; Coombs and Cox 1991), but were less deeply buried, and associated sandstones and tuffs are in general of lower grade. The purpose of this study is to investigate the glass-to-smectite alteration, the transformation of smectite to illite and the relations between morphology and structure of I/S among interbedded bentonites, analcimized tuff and siltstones. These relations in turn demonstrate that factors other than burial depth and temperature are important in determining the grade of diagenesis and very low-grade metamorphism, and that reaction rates are in part dependent on factors associated with specific rock types. They also lead to new insights into the reaction mechanism for the smectite-to-illite transition in bentonites and of significant interlayer composition relations for smectite.

## GEOLOGY AND SAMPLE DESCRIPTION

Near Kaka Point on the southeast coast of Otago, New Zealand, is a northward-younging Middle Triassic marine sequence >1.5 km thick of siltstones and subordinate volcanogenic sandstones. The section contains over 300 thin interbedded ash beds (Coombs et al. 1959; Coombs and Cox 1991). These range from a few mm to a few dm in thickness. Three main types may be distinguished. One type is bentonitic, commonly containing crystal clasts near the base and relict heulanditized glass shards. A second type of tuff alteration is represented on the promontory of Kaka Point by thicker crystal vitric tuffs with considerable heulandite or analcime after glass. The third type consists of cherty or porcellaneous rocks in which original glass shards are replaced by analcime associated with fine-grained quartz and phyllosilicates. Smectite- and heulandite-rich ash beds may pass laterally into analcimized tuffs (Coombs 1965). Evidence has been given by Boles (1971) and Boles and Coombs (1975) that the analcime-quartz assemblage replaced a heulandite precursor via low-temperature fluids with high $Na^+/H^+$ ratios. Ahn et al. (1988) concluded that temperature did not exceed the range 50–100 °C in the Kaka Point block.

The bentonite sample described in this study (D21.6/OU 52329) represents the first type of altered tuff, as described above. It was collected from the Tilson Siltstone, near the top of the Etalian Stage, Middle Triassic, approximately 700 m north of Kaka Point promontory. The bed is about 10–20 cm thick, with thin silty laminae containing clasts of fresh, unaltered plagioclase and quartz about 60 μm in diameter together with numerous relicts of cuspate glass shards, some reaching 0.2 mm in size. Microprobe analyses show that the feldspars are mostly $An_{58-28}$, with a few grains of sodic oligoclase and of alkali feldspar close to $Or_{70}Ab_{30}$. The glass shards are largely replaced by K-rich, Si-rich heulandite ranging into clinoptilolite. The matrix contains very fine-grained aggregates of clay minerals and small cubic crystals and framboids of pyrite (Ahn et al. 1988).

Two siltstone samples were chosen for comparison with bentonite. One (D62/OU 62133) was collected about 100 m above the base of the upper Middle Triassic Port Molyneux Siltstone, about 200 m above the bentonite (D21.6). The other (KP24/OU 62131) was collected about 80 m below the top of the Tilson Siltstone, within a few tens of m of sample D21.6. This is a bioturbated dark siltstone with light-colored sandy laminations. Both siltstones contain clasts of quartz; plagioclase feldspar; abundant intermediate to felsic fine-grained volcanic lithics up to about 100 μm or more in diameter in finely sandy regions; flakes of biotite, chlorite and less abundant muscovite; and patches of cubes or isolated microframboids of pyrite. Siltstone KP24 also contains trace amounts of heulandite.

## METHODS

XRD data were obtained for powdered bulk rocks, using a Philips automated diffractometer with graphite monochromator and Cu$K\alpha$ radiation (35 kV and 15

https://doi.org/10.1346/CCMN.1997.0450106 Published online by Cambridge University Press

mA), with quartz as an internal standard. A step size of 0.005 °2θ and a long counting time of 6 s/step were used to enhance smectite and I/S peaks.

Polished thin sections were prepared with their surfaces approximately normal to bedding so that the optimum orientation could be obtained for optical and SEM observations of textural relations, and so that the (001) planes of phyllosilicates would be preferentially oriented parallel to the beam for TEM observations. SEM observations were made using back-scattered electron (BSE) imaging and X-ray energy dispersive spectral (EDS) analysis with a Hitachi S-570 scanning electron microscope operated at 15 kV. Following SEM observations, 3-mm diameter aluminum washers were attached to selected areas of thin sections. After detachment from the slides, these washer-mounted samples were ion-thinned and carbon-coated for TEM observations. In order to prevent the collapse of smectite layers (from 14 to 10 Å) in the high-vacuum environment and to differentiate smectite layers from illite layers, some samples were treated with L.R. White resin (Kim et al. 1995) prior to TEM sample preparation. TEM observations and AEM analyses were obtained using a Philips CM12 scanning transmission electron microscope (STEM) fitted with a Kevex Quantum solid-state detector and computer system. The STEM was operated at an accelerating voltage of 120 kV and a beam current of ~10 nA to obtain TEM images and selected area electron diffraction (SAED) patterns. AEM quantitative chemical analyses were obtained using the standards muscovite (K, Al), clinochlore (Mg, Al, Fe), albite (Na, Al), fayalite (Fe), rhodonite (Mn, Fe, Ca) and titanite (Ti, Ca) in the thin-foil approximation (Cliff and Lorimer 1975) to derive *k*-ratios, which were utilized to produce concentration ratios from EDS data.

## EXPERIMENTAL RESULTS

### X-ray Diffraction Data and SEM Observations

XRD patterns of bulk rock samples of bentonite show the presence of quartz, plagioclase, heulandite, abundant smectite with randomly interstratified illite/smectite and a subordinate 7-Å phyllosilicate. In order to differentiate between I/S and smectite, XRD data were obtained for both air-dried and glycolated samples. An intense and sharp 11.51-Å peak corresponding to (001) of mixed-layer I/S was observed for the air-dried sample. This peak shifted to 16.19 Å after glycol treatment. Based on the method of Watanabe (1981), the bentonitic sediment is estimated to consist primarily of smectite-rich R0 I/S with approximately 35% randomly interlayered illite. A small peak at about 10 Å was also present both before and after glycolation, reflecting the presence of a small proportion of detrital mica.

The minerals detected in siltstones by powder XRD include quartz, plagioclase, chlorite and 10-Å mica-type phyllosilicates. The powder XRD pattern of air-dried siltstone sample D62 gave quite sharp 14-Å, 10-Å and 7-Å peaks of phyllosilicates, the 7-Å peak being more intense than the 14-Å peak. There is a barely perceptible, very broad peak near 16 Å after glycolation, implying that there may be, at most, trace amounts of smectite. The powder XRD pattern of an air-dried sample of siltstone KP24 also displays sharp 10-Å and 7-Å peaks and a broad 14-Å peak. After glycolation, a weak, broad peak at about 16 Å was observed, suggesting the presence of a very small proportion (<10%) of smectite. There is therefore a range of smectite contents from nil to <10% in the siltstones.

SEM observations show that the bentonitic sediment consists of a small proportion of large detrital grains (>10 μm) consisting largely of quartz, plagioclase, altered glass shards and some chlorite-mica stacks (intergrowths of chlorite and white mica) that have replaced detrital biotite (Li et al. 1995). The detrital grains are surrounded by a matrix of fine-grained clay-like minerals. EDS analyses of this matrix clay suggest the presence of major Si and Al with minor K, Ca, Fe and Mg, consistent with smectite and I/S. Other visible matrix minerals are quartz, albite, pyrite and apatite. There is no strongly preferred orientation of minerals observed in the bentonite.

### TEM Observations

BENTONITE. TEM images show that the matrix phyllosilicates in bentonitic sediment from Kaka Point are composed mainly of smectite-rich mixed-layer I/S, plus subordinate berthierine with 7-Å periodicity (see below for descriptions). Dioctahedral phyllosilicates consist of 2 clay minerals that were characterized in the following ways: The dominant one is smectite, which is characterized by discontinuous, wavy layers with spacings from 10 to 13 Å, depending on the degree of dehydration and layer collapse caused by interaction with the electron beam or by the TEM vacuum. SAED patterns show only diffuse low-order 001 reflections, and AEM analyses have characteristically low interlayer charges. Layer terminations (dislocations) are common and contrast varies markedly along individual layers and between layers. A minor proportion of dioctahedral clay is identified as illite, which is generally characterized by relatively straight, continuous and defect-free (001) fringes having 10-Å interlayer spacings, a characteristic mottled appearance, SAED patterns consistent with a disordered but partially coherent $1M_d$ polytypic sequence and AEM analyses having high Al/Si ratios and interlayer charges. Dioctahedral clay with properties and appearance intermediate between those of smectite and illite is mixed-layer I/S, mostly R0 I/S, although R1 I/S occurs locally. The latter displays alternating dark and light

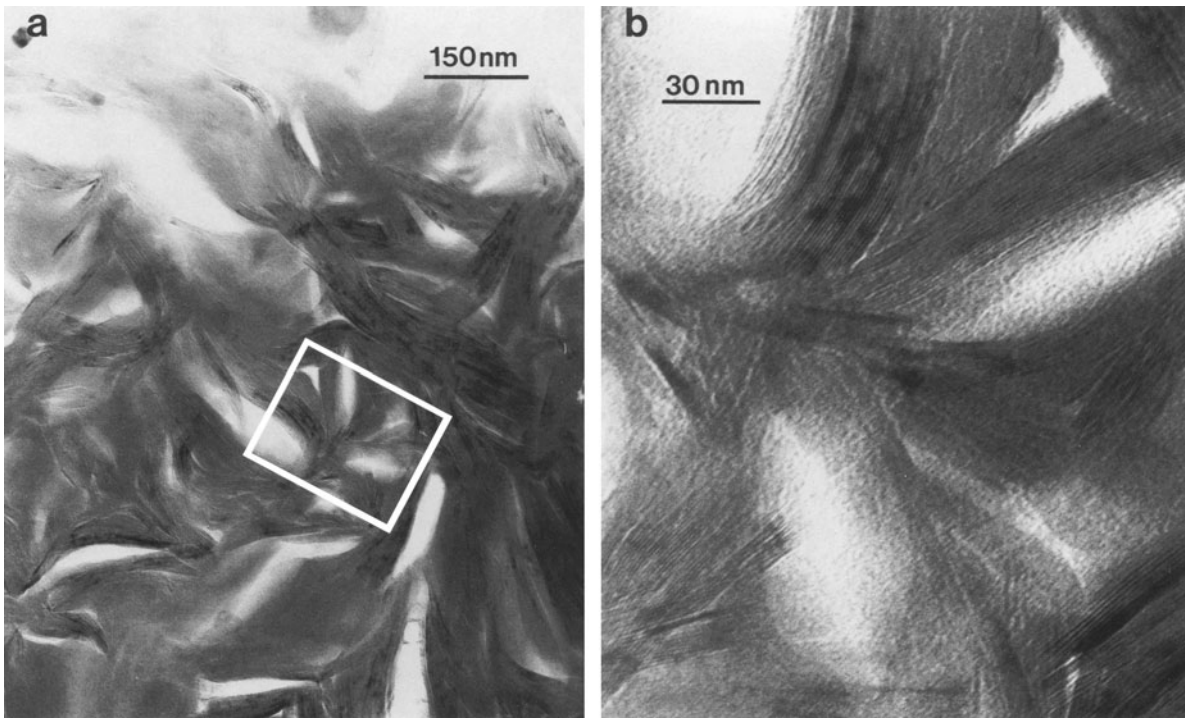


Figure 1. a) Low magnification TEM image of smectite-rich bentonitic sediment showing curved and lens-shaped packets of smectite layers. b) An enlargement of a part of Figure 1a showing smectite lattice fringes.

fringes under proper focus conditions, having 21-Å periodicity. SAED patterns and AEM analyses (illite-like composition) are consistent with this interpretation (Jiang, Peacor et al. 1990). Fringes in R0 I/S are identified as corresponding to either illite-like or smectite-like interlayers by their characteristic thicknesses in samples expanded with L.R. White resin, or by contrast differences where focus conditions were favorable. The proportion of mixed-layer I/S is much larger than that of illite in R0 I/S.

Smectite occurs as discontinuous anastomosing layers enveloping the relatively large detrital grains, and exhibits a typical curved (sometimes circular or semicircular) lens-shaped morphology in TEM images, with no preferred orientation (Figure 1a). Although samples not treated with L.R. White resin damaged easily, lattice fringe images of minimally damaged smectite display randomly oriented 10- to 11-Å wavy or curved layers resulting from collapse of 14-Å layers in the high vacuum environment (see Figure 1b, which is an enlargement of part of Figure 1a). In images of ion-milled samples that were permanently expanded with L.R. White resin, smectite displays anastomosing layers having 10.5- to 13-Å interlayer spacings with a high density of edge dislocation-like layer terminations (indicated by white arrows in Figure 2). In some areas, smectite occurs as thin packets that are oriented at relatively large angles to one another. Curved packets of smectite with a discontinuous circular shape were commonly observed to surround relatively featureless cores. Those cores gave no SAED patterns, implying that they are either non-crystalline or so rapidly beam-damaged that SAED patterns cannot be obtained rapidly enough. However, AEM analyses were very similar to those of smectite (see below), and unlike those typical of volcanic glass or heulandite. We therefore infer that such cores consist of a poorly ordered precursor to crystalline smectite, akin to materials observed by Masuda et al. (1996) for glass undergoing alteration in Nankai Trough bentonites. The boundary between materials was commonly observed to be sharp (as in the upper part of Figure 3a), but in other areas there is no discernible boundary between enveloping smectite and the enclosed core (as in the lower part of Figure 3a). Such structures demonstrate that the enveloping smectite has altered directly from glass shards, as represented by the relict cores.

Away from the smectite/glass boundaries, lattice fringes of dioctahedral phyllosilicate are less anastomosing and wavy and have 10- to 11-Å spacings that sometimes display mixed-layer I/S contrast. However, the curved texture of the smectite packets is generally preserved in such mixed-layer I/S packets. AEM analyses of such material yield chemical compositions between those of smectite and illite, indicating mixed-layer I/S. These textural and chemical relations suggest a general trend of increasing illite component in mixed-layer I/S from the envelopes around relict glass

https://doi.org/10.1346/CCMN.1997.0450106 Published online by Cambridge University Press


Figure 2. TEM lattice fringe image of permanently expanded bentonite showing that smectite occurs as imperfect and anastomosing layers having a 10.5- to 13-Å interlayer spacing with numerous edge dislocation-like layer terminations (indicated by white arrows).

shard-like material to more clay-rich areas in bentonitic sediments. For example, Figure 3b shows that the curved, defect-rich smectite layers (with 10.5- to 13-Å spacings) occur around the altered glass shard-like material and that the smectite changes to randomly disordered R0 I/S layers having 10- to 11-Å spacings away from the altered glass shard-like material. Lattice fringes are anastomosing and wavy, near altered glass shard-like material, but layers become straighter away from the altered glass shard-like material. Although the dominant dioctahedral clay occurs as thin packets of smectite-rich R0 I/S, which have different kinds of fringe contrast and for which the fringe spacings are variable, some lattice fringe images show local ordering of R1 I/S (Figure 4). The inset SAED pattern shows relatively irregular, intense 001 reflections ($d \approx$ 10.5 Å and submultiples) superimposed on rather diffuse reflections and streaking along **c***, suggesting a mixture of smectite and I/S, primarily a randomly disordered R0 I/S. The diffuseness and irregular non-periodicity of reflections in non-001 rows are consistent with a partially coherent, but largely disordered stacking sequence. Although representing only partial disorder, such sequences have been labeled as $1M_d$ (Grubb et al. 1991).

Figure 5 is typical of smectite-rich I/S occurring as stacks of curved packets of anastomosing layers. In the middle part of the lattice fringe image, wavy smectite layers are observed closely associated with mixed-layer I/S layers, which show different fringe contrast and layer spacings. The white arrow indicates where 3 layers of smectite appear to transform to 4 layers of I/S, with preservation of the original curved texture. Similarly, packets of mixed-layer I/S were commonly observed to have layer curvature that is typical of smectite, as consistent with replacement of smectite by I/S.

Figure 5 also shows thin packets of 7-Å layers intergrown with smectite-rich I/S. AEM analyses indicate that the 7-Å phyllosilicate is berthierine with a very high Fe/Mg ratio. It was always observed to be closely associated with mixed-layer I/S, but never with the smectite-rich clays surrounding the relict glass shards. Berthierine was the only trioctahedral clay mineral observed in the matrix; i.e., no chlorite was detected. The occurrence of berthierine as a metastable precursor to chlorite (Ahn and Peacor 1986) is consistent with the early stage of diagenesis as represented by smectite-rich material and with a highly reducing environment which is compatible with the framboidal pyrite.

In other areas, relatively wavy fringes of mixed-layer I/S with 10- to 11-Å spacings and typical variable contrast are associated with very thin packets (3 to 6 layers) of locally straight and defect-free illite-like layers having only 10-Å spacings. The fringe contrast of mixed-layer I/S is observed to disappear at the boundary between mixed-layer I/S and illite-like layers. Sequences of mixed-layer I/S fringes sometimes display sharp along-layer changes to straight illite layers, and the I/S and illite layer sequences may be parallel or subparallel. The boundaries between mixed-layer I/S and illite are indicated by white arrows in Figure 6. Such along-layer changes are consistent with direct replacement of one kind of layer by another. The fringes of illite exhibit fewer edge dislocation-like layer terminations than those of smectite-rich I/S. The inset SAED pattern in Figure 6 is like that of I/S (labeled as corresponding to $1M_d$), implying stacking sequences like those of I/S.

Clay separates were also observed as grains dispersed on holey carbon grids, so that **c*** was preferentially parallel to the electron beam. TEM images (Figure 7a) of clay particles display irregular cornflake-like morphology with curved edges that are typical of smectite found in bentonites having low porosity and permeability (Nadeau et al. 1985; Inoue et al. 1990). No euhedral crystal outlines were observed. Some flakes exhibit rounded morphology, suggesting dissolution of primary smectite (Figure 7a). EDS anal-

https://doi.org/10.1346/CCMN.1997.0450106 Published online by Cambridge University Press

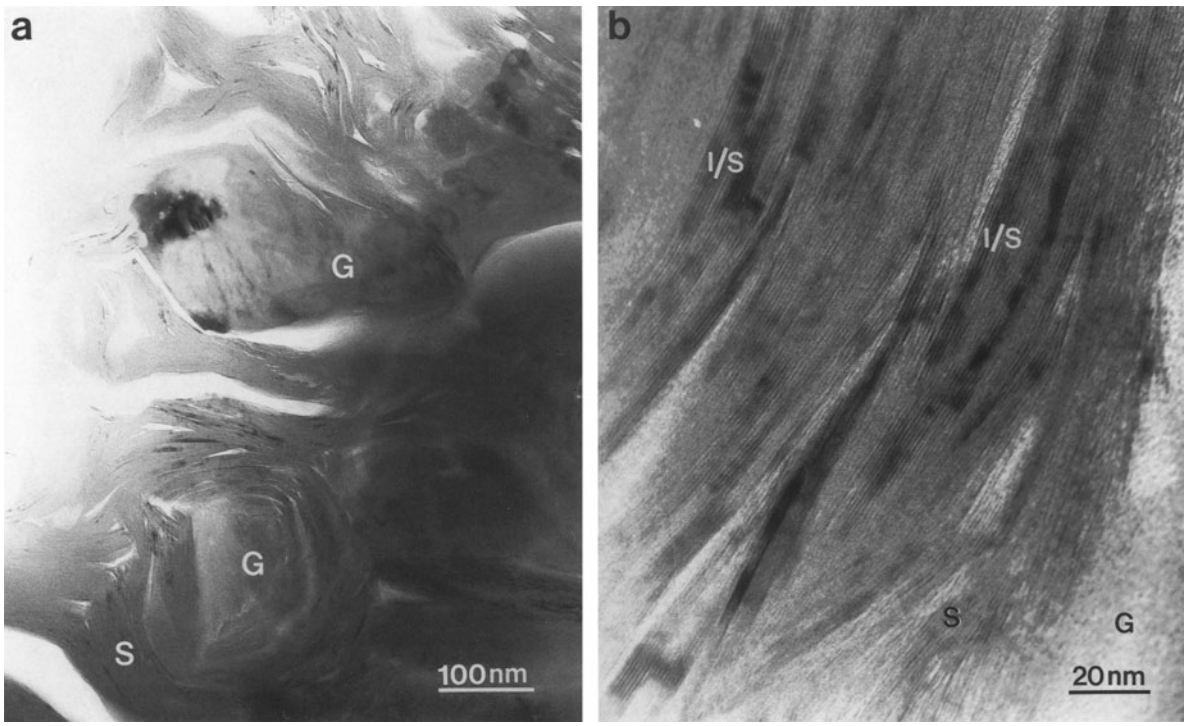


Figure 3. a) TEM image of bentonite showing altered glass shard-like material (G) and surrounding packets of smectite (S) or smectite-rich I/S of curved layer. Note that there is no apparent boundary between the central material and surrounding smectite in the lower part of the picture. b) Lattice fringe image showing that imperfect smectite occurs around altered glass shard-like material, whereas smectite changes to mixed-layer I/S away from altered glass shard-like material.

yses (see below), were consistent either with nearly pure smectite or more illite-rich I/S, as indicated by Al and alkali contents. SAED patterns with *hk*0 reflections typically display 2 types of pattern: One has more-or-less continuous rings with superimposed spots, essentially corresponding to a powder pattern caused by random rotation of layers about **c***; that is, layers are dominantly turbostratically-related, but with local coherency. EDS analyses correspond to smectite. The second type of pattern, corresponding to mixed-layer I/S, displays a sequence of sharp reflections in place of the more-or-less continuous circles of the first type. Such patterns are consistent with coherency between layers in thin sequences, such packets being related by incoherent boundaries and random rotations (Figure 7b).

SILTSTONES. In contrast to the bentonite, TEM images of the matrix clay in siltstones consist mainly of 10-Å illite and 14-Å chlorite. The lattice fringes of illite are generally straight, continuous and defect-free (Figure 8a). Layer terminations (dislocations) are rarely observed in the (001) fringes. The crystals of illite have a platy subhedral shape and the discrete packets are thicker (up to 300-Å) than those of smectite or I/S *in* bentonite. The SAED patterns of most illite crystals display $1M_d$ polytypism, but some thicker crystals consist of the $2M_1$ polytype. Only a minor proportion of matrix dioctahedral clay is characterized as having slightly wavy lattice fringes and rarely displaying contrast variations typical of R1 mixed-layer I/S. Such material always has $1M_d$ polytypism and is identified as mixed-layer I/S. AEM analyses indicate that dioctahedral clays in the siltstones have 6.7 to 7.1 Si pfu and 1.0 to 1.4 K pfu as interlayer cations. No Na was detected. No smectite was observed by TEM in the matrix. Chlorite occurs as well-defined packets of layers that are very closely associated with illite (Figure 8b). The (001) interfaces of chlorite may be parallel or subparallel to those of illite. Chlorite crystals also display a platy subhedral shape. No 7-Å berthierine was identified intercalated in packets of matrix phyllosilicates. However, TEM lattice fringe images of detrital biotite flakes display various alteration phenomena, including transformation of 10-Å biotite layers to 7-, 14- and 24-Å layers, indicating that biotite has been partially altered to various phyllosilicates such as 7-Å berthierine, 14-Å chlorite, 24-Å corrensite and mixed-layered chlorite and saponite. This observation is consistent with the strong 7-Å peak (berthierine) and a small smectite component in the bulk powder XRD patterns.

## AEM Analyses of Bentonite

AEM analyses were carried out only for smectite- and I/S-rich areas that were first observed in TEM

https://doi.org/10.1346/CCMN.1997.0450106 Published online by Cambridge University Press

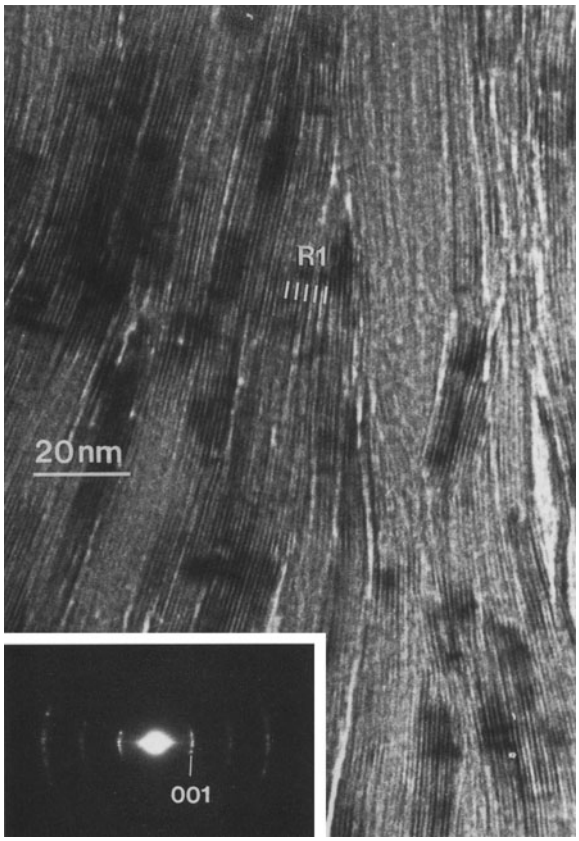


Figure 4. Lattice fringe image of smectite-rich I/S in bentonite showing local ordering of I/S having R1 units. The packets of layers display numerous layer terminations. The inset diffraction pattern indicates a disordered $1M_d$ polytype.

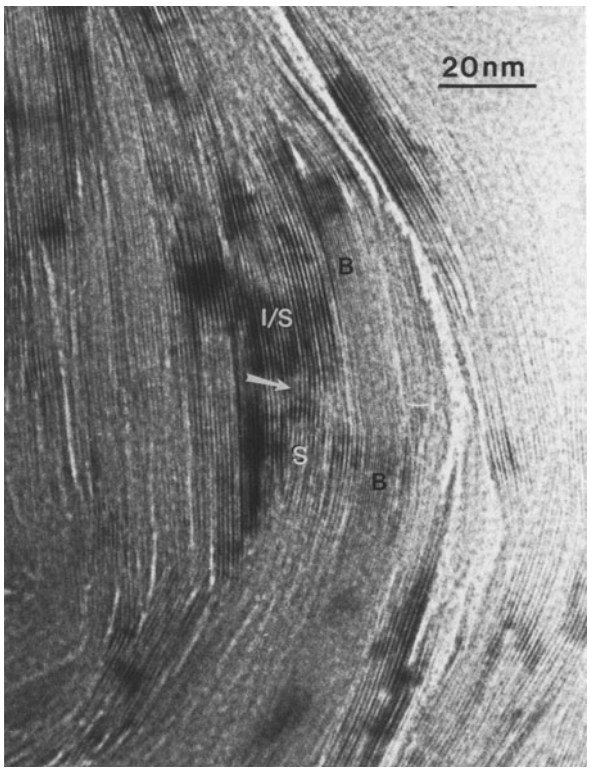


Figure 5. TEM lattice fringe image of bentonite showing transformation of 3 smectite layers (S) to 4 I/S layers (indicated by a white arrow). A thin packet of 7-Å berthierine (B) is closely associated with smectite-rich I/S.

images to be homogeneous over areas larger than 10 nm in diameter and that displayed the typical textural characteristics described above. All AEM analyses for smectite were obtained from circular packets enclosing altered glass shard-like material; those for I/S were obtained for material that displayed I/S-like contrast and were not associated with relict shards. AEM data for smectite and mixed-layer I/S are listed in Table 1. The values for Si and Al contents are distinctly different for smectite and I/S, although both have wide ranges. Si and Al contents of smectite appear to vary more widely than in mixed-layer I/S. Larger Al and smaller Si contents are typical of more illite-rich material. The Fe and Mg contents of smectite are also greater than those of I/S. Such differences are typical of reactant smectite and product illite as shown by Ahn and Peacor (1986) for Gulf Coast mudstones. The difference in Mg and Fe contents is ascribed to formation of chlorite or berthierine (Hower et al. 1976). The association of berthierine only with more illite-rich material in samples of this study is consistent with that relation.

The smectite is characterized as having K as the dominant interlayer cation. The Na content varies from being undetectable to approximately equal to that of K, the ratio of Na/(K+Na+Ca) varying from 0 to 0.45. Some smectite has small Ca contents. Smectite is generally considered to be Ca- or Na-rich, large interlayer K contents being thought to be typical only of illite. However, the high K contents of this study were obtained from areas not showing illite-like layers, and the smectite identification is confirmed by the characteristic Si/Al ratios. The K content of mixed-layer I/S (Table 1) is significantly larger than that of smectite, as expected. No Ca was detected in I/S, and the Na content is substantially smaller, with Na/(K+Na+Ca) ranging from 0 to 0.20. The smectite has a range of interlayer site occupancy from 0.60 to 0.87 pfu, whereas I/S has a range of 0.94 to 1.21 pfu, the latter being very close to those of illite (Jiang et al. 1992).

Table 1 also lists data from representative AEM analyses of the trioctahedral phyllosilicate berthierine that coexists with mixed-layer I/S. Both analyses have large Fe/(Fe+Mg) ratios (0.76–0.80), which is characteristic of berthierine relative to the smaller values typical of chlorite. The small amounts of Ca and K are inferred to be caused by contamination with sur-

https://doi.org/10.1346/CCMN.1997.0450106 Published online by Cambridge University Press

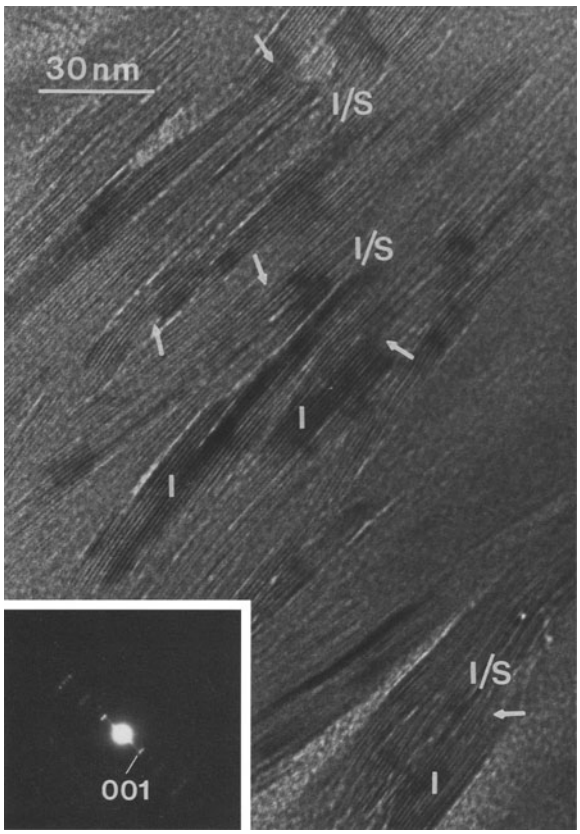


Figure 6. TEM lattice fringe image of bentonite showing that relatively wavy mixed-layer I/S layers are closely associated with locally straight illite-like layers. Mixed-layer I/S layers transform to illite-like layers (I) (indicated by white arrows). The inset SAED pattern suggests a $1M_d$ polytype.

rounding minerals, as analyzed grains were as small as 100 Å in thickness.

## DISCUSSION

### Overview

The XRD, SEM and TEM/AEM data show that the bentonite consists primarily of smectite-rich I/S with approximately 35% randomly interlayered illite, associated with packets of subordinate berthierine. The illite is generally randomly interlayered with smectite, but there is local ordering, primarily of R1 type. Relatively uncommon material with the appearance of altered glass shards gives no SAED pattern but has a composition like that of smectite. Numerous other small glass shards have been replaced by K-rich heulandite or clinoptilolite. The remnants of shards are encircled by envelopes of curved smectite layers, but there is no illite interlayered with the smectite. These relations collectively imply a sequence of reactions in bentonite: 1) alteration of glass to a smectite "precursor"; 2) long-range ordering of the precursor to smectite; 3) formation of I/S through transformation of at least some smectite.

### Formation of Smectite from Glass in Bentonite

The alteration of glass through a non-crystalline (i.e., non-long-range-ordered) precursor to clay has been observed in several studies, although not in material of the relatively great age of those of this study. For example, in their experimental work on hydrothermal alteration of volcanic glass, Kawano and Tomita (1992) observed that noncrystalline flaky and/or fibrous materials formed first as reaction products, and that the flaky and/or fibrous materials subsequently curled inward and transformed into smectite having a circular outline. In other studies, transitional, noncrystalline spheres were observed to transform to a smectite precursor material and then to smectite with layers originally parallel to sphere surfaces (Eggleton and Keller 1982; Tazaki et al. 1989). Masuda et al. (1996) studied the alteration of glass to smectite in bentonite from a sequence of core samples obtained in the Nankai Trough. They found that a primitive, non-crystalline precursor to smectite forms with a layered structure curved to the surface of glass shards. Such material evolves to crystalline smectite whose layers curve into spherical shapes, then change to smectite occurring as packets of layers subparallel to bedding. The resulting layers have no apparent relation to the original shard shapes.

The sequence observed by Masuda et al. (1996) in progressively deeper core samples is similar to that observed in different areas of the single bentonite sample of this study. TEM images of the remnant shard cores are relatively homogeneous and featureless, like glass. However, they have a composition near that of smectite (as observed by Masuda et al. 1996 for the smectite precursor), implying that such material must be ordered on a short-range basis. Although similar non-crystalline precursor materials were observed in the studies noted above, such materials were obtained either in experiments or on samples in which processes occurred recently. Survival of such disordered material over long periods is apparently implied by the Triassic age of the samples studied here, although some long-range order may not have been observed because of rapid damage caused by the electron beam.

COMPOSITION OF SMECTITE INTERLAYERS. The AEM data show that the interlayers of the smectite derived directly as an alteration product of glass shards have an interlayer composition dominated by K, even though no illite-like layers were detected. In some cases, the Na content approximates that of K, and small amounts of Ca are present, but K is generally present in amounts much greater than those of either Na or Ca. The same applies to the associated heulandite which replaces glass shards, as shown by electron micropro-

https://doi.org/10.1346/CCMN.1997.0450106 Published online by Cambridge University Press

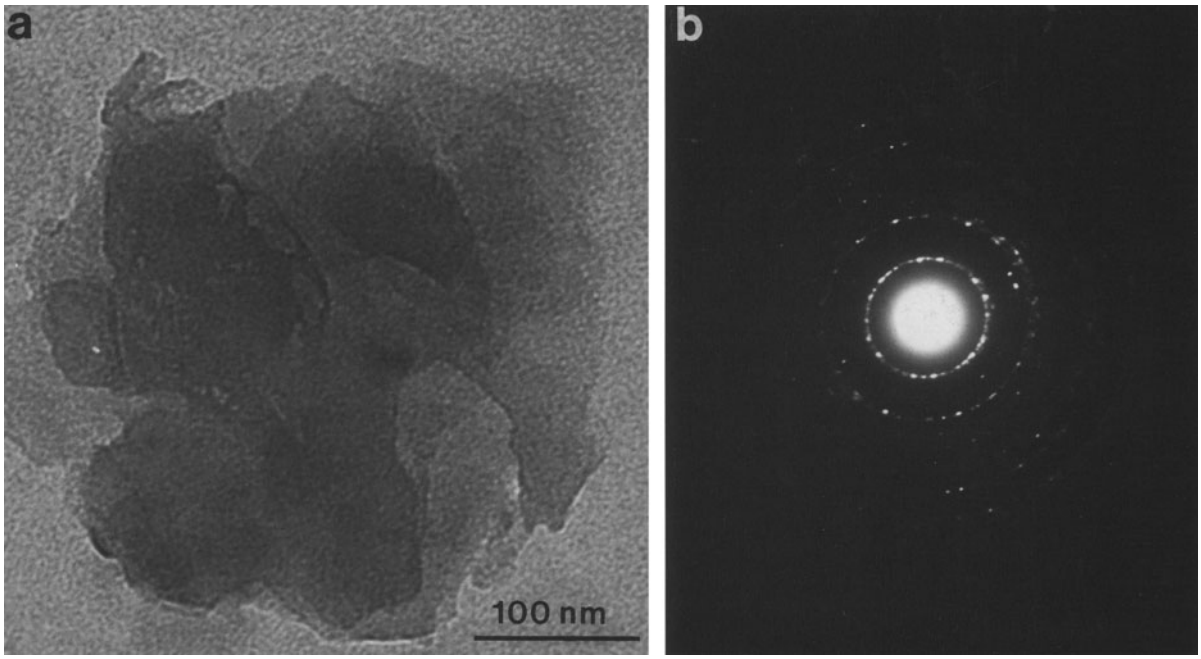


Figure 7. a) TEM image of irregular smectite-rich I/S flakes from the clay fraction of bentonite showing the typical "corn flake" texture. Some flakes exhibit rounded morphology, suggesting dissolution of primary smectite. b) Selected area electron diffraction pattern for (*hk*0) reflections of smectite-rich I/S in Figure 7a showing well-defined spots, implying dominant random orientation of layers about **c***, but with some coherence of layers in packets.

be analyses. These results are compatible with a whole-rock analysis of a Kaka Point bentonite (Boles and Coombs 1975, Table 1) which shows CaO 0.75%, $Na_2O$ 2.20%, $K_2O$ 3.30% with much of the CaO and $Na_2O$ being attributable to heulandite and any detrital plagioclase clasts.

It is generally thought that smectite interlayers are characterized by high Na or Ca contents, and illite by high K (or Na) contents. However, smectite having K as the dominant interlayer cation has recently been reported as occurring in many sites, including Gulf Coast mudstones (Freed and Peacor 1992), Barbados accretionary wedge bentonites (Buatier et al. 1992), mid-Atlantic Ocean bentonites (GR Dickens, personal communication, 1994), Nankai Trough bentonites (Masuda et al. 1996), altered mid-oceanic-ridge basalt (Shau and Peacor 1992) and marine muds of the Mississippi Delta (Hover et al. 1995). The AEM data of this study further confirm this trend, the collective data implying that smectite in marine sediments, in contrast to that of the weathering environment, generally has K as the dominant interlayer cation.

## The Smectite-to-Illite Transition in Bentonite: Local Dissolution and Crystallization

TEM data show that the earliest-formed smectite occurs as packets of curved layers that conform to the shapes of relict glass shards, often with no discernible boundary. However, where no glass shards are now present, the clay mineral is smectite-rich R0 I/S, but with some locally ordered R1 I/S (50% illite). As seen in many TEM lattice fringe images, packets of mixed-layer I/S commonly preserve the curved morphology and lens-like shape of packets of earliest-formed smectite. Most importantly, small numbers of contiguous layers of R0 and R1 I/S were observed to change along-layer to illite, implying that a transition was incomplete. The increase in illite component is confirmed by AEM data, which show that the composition of the R0 I/S approaches that of illite (or R1 I/S) with increasing illite component. These observations suggest that mixed-layer I/S formed by direct replacement of layers of original smectite.

Direct replacement of layers of one clay mineral by another has been observed in many studies. For example, Ahn and Peacor (1987) observed 2 textural relations in the same sample, that is, common replacement of one layer of biotite by 2 kaolinite layers, and of thick packets of biotite layers by packets of kaolinite layers. Only along-layer transitions between 1 biotite layer and 2 kaolinite layers were observed, and they proposed that the interface between such kaolinite and biotite layers served both as an advancing reaction front and a defect along which water and reactant and product ions could diffuse. Such relations are often referred to as being "solid state" because of the close relation between product and reactant structures (Veblen 1992), a relation common to all replacements

https://doi.org/10.1346/CCMN.1997.0450106 Published online by Cambridge University Press

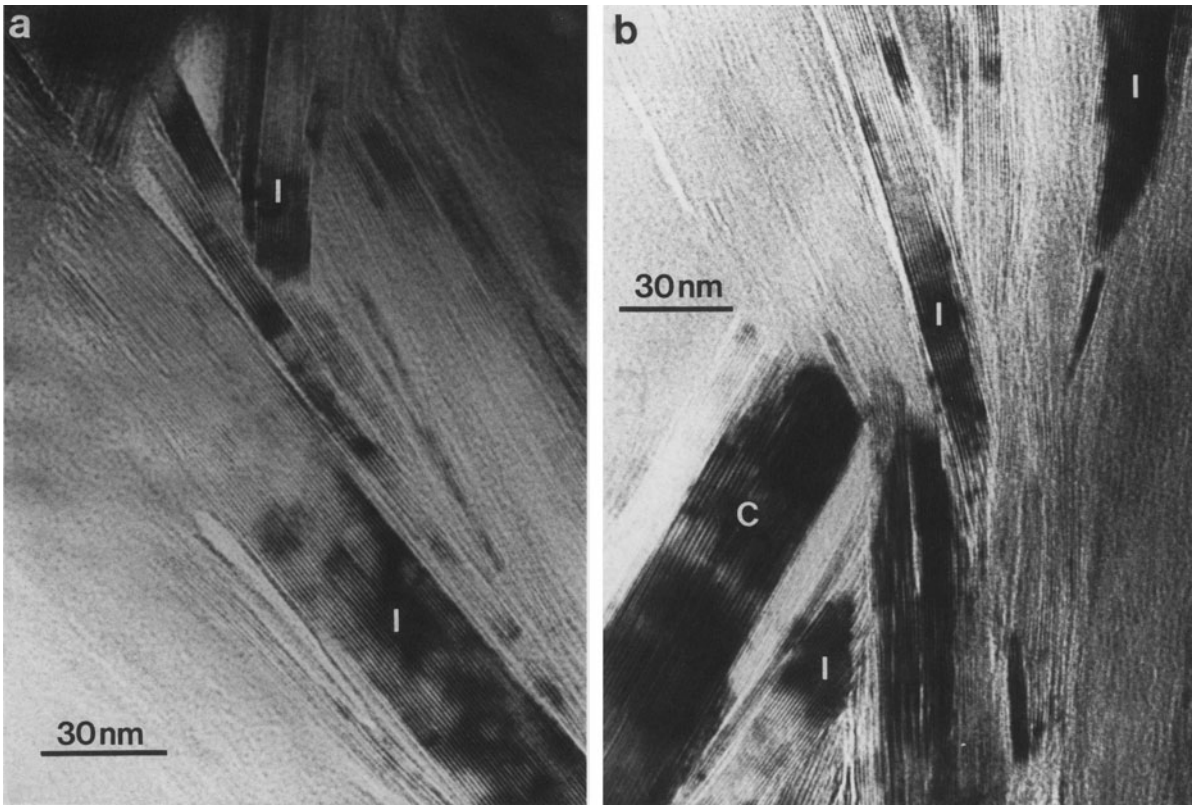


Figure 8. TEM lattice fringe images of clay minerals in siltstone. a) Illite (I) crystals have straight, regular and continuous (001) layers. The crystals occur as distinct packets with platy subhedral shapes. b) TEM lattice fringe image showing intergrown illite (I) and chlorite (C) crystals. The chlorite also occurs as discrete subhedral packets.

where phyllosilicates are both reactants and products. However, the reaction is necessarily mediated by a fluid and involves dissolution of one phase (such as smectite) and crystallization of another (such as I/S or illite), albeit over a volume whose dimensions are on the order of magnitude of Å. The term "solid state" must therefore be used cautiously, as it does not imply lack of an essential "fluid", even although that "fluid" may be only a few unit cells thick with properties modified by bonding to the adjacent solid surfaces.

That the replacement of smectite by I/S or illite is locally one of dissolution and crystallization is implied by several relations. Most importantly, the compositions of reactant smectite and product illite are different, not only in interlayer cations but in both octahedral and tetrahedral cations. As pointed out by Ahn and Peacor (1986), such differences cannot arise via solid state diffusion, but are the natural result of dissolution and crystallization, in part simply because the rate of diffusion of octahedral and tetrahedral cations in phyllosilicates is very low. Furthermore, the occurrence of berthierine, which presumably forms in part from the Fe and Mg arising through the lower Fe and Mg components of illite relative to smectite, is an obvious result of dissolution, mass transport and neocrystallization. However, the significant differences in SAED patterns are consistent with limited coherency in I/S and illite, whereas the smectite appears to be dominated by turbostratic stacking. Changes in relative orientations of layers, in terms of rotation about **c***, are consistent with dissolution and crystallization, but not solid-state diffusion, in the strict sense. Furthermore, the number of layers across boundaries marking along-layer transitions were often observed to be different; for example, 4 I/S layers changing to 5 illite layers, requiring that at least some dissolution or neocrystallization took place.

Yau et al. (1987) emphasized the role of water/rock ratio in determining the textures resulting from the smectite-to-illite transition. In porous, open systems, dissolution may occur on a massive scale, with transport of dissolved components to distant sites where direct crystallization occurs. As in sediments of the Salton Sea Geothermal Field (Yau et al. 1987) or in hydrothermal systems (Inoue et al. 1987), euhedral crystals of illite result. By contrast, in impermeable rocks with low water/rock ratios, dissolution and crystallization may occur on scales as small as individual layers, or, as is commonly the case, via very thin packets of layers. Reactions progress "along layers" until

Table 1. Normalized AEM data for smectite, illite/smectite, and berthierine in sample D21.6.†‡

| | Smectite | | | | | Illite/smectite | | | | | Berthierine | |
|---|---|---|---|---|---|---|---|---|---|---|---|---|
| | 1 | 2 | 3 | 4 | 5 | 6 | 7 | 8 | 9 | 10 | 11 | 12 |
| Si | 7.24 | 7.33 | 7.34 | 7.80 | 7.48 | 7.17 | 7.07 | 7.11 | 6.96 | 6.94 | 6.29 | 5.71 |
| $Al^{IV}$ | 0.76 | 0.67 | 0.66 | 0.20 | 0.52 | 0.83 | 0.93 | 0.89 | 1.04 | 1.06 | 1.71 | 2.29 |
| $Al^{VI}$ | 2.84 | 2.79 | 2.64 | 2.91 | 2.89 | 3.11 | 3.36 | 3.16 | 3.23 | 3.37 | 3.66 | 3.28 |
| $Fe^{2+}$ | 0.60 | 0.76 | 0.80 | 0.57 | 0.64 | 0.41 | 0.30 | 0.47 | 0.41 | 0.34 | 5.35 | 6.32 |
| Mg | 0.56 | 0.45 | 0.54 | 0.52 | 0.47 | 0.46 | 0.34 | 0.37 | 0.36 | 0.29 | 1.74 | 1.63 |
| Mn | n.d.§ | n.d. | 0.02 | n.d. | n.d. | 0.02 | n.d. | n.d. | n.d. | n.d. | 0.14 | 0.15 |
| Ca | 0.08 | n.d. | n.d. | 0.06 | 0.11 | n.d. | n.d. | n.d. | n.d. | n.d. | n.d. | 0.06 |
| Na | n.d. | 0.25 | n.d. | 0.33 | 0.30 | 0.13 | 0.16 | n.d. | n.d. | 0.06 | n.d. | n.d. |
| K | 0.68 | 0.65 | 0.60 | 0.34 | 0.47 | 0.79 | 0.99 | 1.21 | 1.13 | 0.98 | 0.27 | 0.13 |
| Total cations | 12.76 | 12.90 | 12.60 | 12.73 | 12.87 | 12.94 | 13.15 | 13.21 | 13.13 | 13.04 | 19.16 | 19.57 |
| Na/(K + Na + Ca) | 0 | 0.28 | 0 | 0.45 | 0.13 | 0.20 | 0.14 | 0 | 0 | 0.06 | 0 | 0 |
| Fe/(Fe + Mg) | 0.52 | 0.63 | 0.60 | 0.53 | 0.58 | 0.47 | 0.47 | 0.56 | 0.53 | 0.54 | 0.76 | 0.80 |

† Normalization is based on 12 cations on tetrahedral and octahedral sites for smectite and I/S, 20 O + 16 (OH) for berthierine. All Fe is assumed to be ferrous.

‡ Two standard deviations on the basis of calculating statistics are 0.05–0.07 pfu for Si, 0.07–0.09 pfu for Al for all analyses; 0.01–0.03 pfu for Fe, 0.01–0.02 pfu for Mg, 0.01–0.04 pfu for Na, 0.01–0.02 pfu for Ca and 0.06–0.13 pfu for K for smectite and I/S; and 0.20–0.25 pfu for Fe, 0.09–0.15 pfu for Mg and 0.01–0.02 pfu for Mn for berthierine, respectively.

§ n.d. = not detectable.

all layers may be replaced. The resulting textures thus appear to be direct replacements, as in most, but not all, of the materials of this study. These 2 cases represent contrasting end members.

Alternatively, Ahn and Peacor (1986) and Buatier et al. (1992) observed euhedral crystals of I/S within a continuous matrix of smectite in Gulf Coast mudstones and bentonites of the Barbados accretionary wedge, respectively. Freed and Peacor (1992) studied authigenic I/S crystals in clay separates of Gulf Coast shales by TEM and AEM, verifying the relations involving euhedral I/S in Gulf Coast samples. Such relations appear to be a hybrid of open- and closed-system models described above.

Much of the controversy regarding mechanisms of the smectite-to-illite transition may arise because the transition mechanism appears to be quite different in different localities. The search for a single, universal mechanism is therefore bound to give rise to apparently inconsistent results. However, all textural relations described here are consistent with a single mechanism at the structural level, i.e., dissolution and crystallization. The essential difference is only in distances over which reactants and products are transported, and in the water-mediated mechanism of ion transport.

## Contrast in the Rate of the Smectite-to-Illite Transition in Bentonite and Other Sediments and its Controlling Factors

The observations of dominant smectite-rich I/S in bentonite of the present study are consistent with XRD data for clay minerals in 17 bentonites throughout the 4.8–8.5 km Triassic section in Hokonui Hills, 100–120 km northwest of the present study area (Boles and Coombs 1975). In a reconnaissance study, Boles and Coombs (1975) found that smectite is the dominant clay mineral in all cases, but with subordinate illite in most samples. Furthermore, they detected no systematic changes in clay minerals with depth of burial. These data collectively suggest that little mineralogical change has occurred in bentonitic sediments subsequent to sedimentation and burial.

The siltstones occurring within 200 m both above and below the bed from which the bentonite sample was collected contain matrix clay minerals consisting mainly of illite and chlorite, with only a very small proportion of mixed-layer I/S. This indicates that insofar as smectite was originally present in the siltstones, its transformation to illite is much more advanced than in bentonites. Similarly, Ahn et al. (1988) studied analcime-rich altered tuff (sample D13.2), which is located within 800 m stratigraphically of the smectite-rich bentonitic sediment (D21.6) described in this study. They found that discrete authigenic illite occurs as relatively thick packets (compared with those of I/S in bentonites) of straight and defect-free 10-Å layers intergrown with discrete packets of chlorite, corrensite and mixed-layer chlorite/corrensite. No smectite or I/S were detected by TEM in the analcimized sample, as is consistent with XRD data. The analcimized tuffs occurring both directly above and below the bed from which the bentonite sample of this study was obtained are mineralogically equivalent to the sample studied by Ahn et al. (1988), as shown in part by XRD data. The analcime-quartz assemblage was inferred to have replaced a heulandite precursor via low-temperature fluids with high $Na^+/H^+$ ratios (Boles 1971; Boles and Coombs 1975; Coombs 1993), implying prograde alteration of the original heulandite- and smectite-rich volcanic ash. Such a lack of correlation between burial depth and mineral assemblages is in contrast with observations at many localities in-

cluding those in Gulf Coast Tertiary sediments, in which a systematic decrease in expandable component of mixed-layer I/S is correlated directly with an increase in burial depth and temperature (Perry and Hower 1970).

These relations imply that the transformation of smectite to illite was substantially retarded in the bentonite of this study relative to siltstones and analcimized tuffs of the same burial depth and age. Similar relations have been observed elsewhere (Sucha et al. 1993; Tribble and Wilkens 1994; Velde 1995), and most notably in the Nankai Trough, where smectite is now in the process of transforming to mixed-layer I/S as the dominant clay mineral in shales at an early stage of diagenesis. However, alteration of volcanic glass in bentonites interbedded with the shales has given rise only to smectite (Masuda et al. 1996). In that case, the difference in reaction rates is not related to differences in the original source of smectite, as the smectite in both bentonites and shales was derived *in situ* from volcanic glass. These data emphasize the significance of factors other than burial depth, temperature and even time in determining the grade of diagenesis and very low-grade metamorphism as measured by the progress of smectite-to-mica reactions.

Many workers have claimed that the extent of progress of the smectite-to-illite reaction can be used to determine the temperature of transition in basin sediments undergoing diagenesis. However, such a direct correlation requires that both illite and smectite be stable phases and that true chemical equilibrium be attained (Essene and Peacor 1995). Jiang, Essene and Peacor (1990) showed that illite (as well as smectite) is a metastable phase. They and other workers (Ahn et al. 1988; Ahn and Peacor 1989; Freed and Peacor 1989; Inoue et al. 1990; Essene and Peacor 1995) have inferred that the extent of the smectite-to-illite transformation is kinetically controlled and therefore governed not only by temperature, pressure and composition, but also by additional factors. Important among these is water/rock ratio (Whitney 1990), activities of interlayer cations, especially K (Huang et al. 1993), the presence of maturating organic matter (Small and Manning 1993; Small 1994), time (Ramseyer and Boles 1986; Pytte and Reynolds 1989; Pollastro 1990) and heating rate (Hillier et al. 1995). Some investigators have implicitly recognized that the progress of reaction of such metastable phases is kinetically controlled by a variety of factors, but that, if all other relevant factors are constrained, then duration or temperature of reaction can be determined (Huang et al. 1993). The specific reason for the lower rate of formation of illite where smectite is a reactant in bentonites relative to shales is unclear. Two possibilities are especially apparent: smaller values of permeability (water/rock ratio) and absence of organic acids. Albitization of detrital plagioclase is also inhibited in fine-grained sediments of low permeability as compared with coarser grained, more permeable rocks (Boles and Coombs 1977).

As shown in TEM images, matrix illite and chlorite crystals occur as discrete packets with subhedral shapes in the siltstones within which bentonite beds occur. Ahn et al. (1988) showed that the analcime-rich rocks are clastic sediments in which discrete packets of illite and chlorite exhibit subhedral crystal shapes, appearing to occupy void space among larger crystals of other minerals. Those relations suggest formation of illite by neoformation. By contrast, the bentonite exhibits a more-or-less continuous array of layers of clay minerals with no suggestion of the void space that must originally have been present. The significantly greater extent of reaction in analcime-rich sediments is therefore compatible with greater water/rock ratio, as consistent with the results of Whitney (1990).

The importance of K availability to the smectite-to-illite reaction has been long recognized from detailed geochemical studies (Hower et al. 1976). Huang et al. (1993) derived an empirical kinetic model from experiments which demonstrates that the illitization rate of Wyoming bentonite is increased with concentration of $K^+$ in pore fluids and that variation of $K^+$ in shale pore fluids can significantly affect the rate of smectite-to-illite transition. Observation of shales of the Precambrian (1.1 Ga) Nonesuch Formation in the vicinity of White Pine copper mine, Michigan, showed that, due to the lack of K availability and other factors, authigenic clays are still mixed-layer I/S with up to 30% smectite despite their great age (Li et al. 1995). Study of mineral relations and major element chemistry of bentonites from ODP site 808 in the Nankai Trough by Masuda et al. (1996) revealed that smectite in bentonites is initially K-rich, but it becomes more Na-rich at the greater depth where clinoptilolite forms. As clinoptilolite becomes increasingly K-rich with depth, the transformation of smectite to illite is inhibited as a result of clinoptilolite behaving as a sink for K (Masuda et al. 1992). The presence of K-rich heulandite or clinoptilolite pseudomorphing the larger glass shards in the Kaka Point bentonites is to be noted in this context.

On the other hand, the rate of the smectite-to-illite transition can also be affected by organic acids, bentonites being poor in organic material, whereas shales are generally noted as sources of organic material. Experiments of Small and Manning (1993) and Small (1994) emphasized the importance of oxalate and acetate ions generated during maturation of hydrocarbons in promoting illitization. Eberl (1993) proposed that the generation of carboxylic acids during maturation may enhance the precipitation of illite by promoting the dissolution of smectite and K-feldspar. Although the observations of this study provide no direct evidence for the significance of organic material in the

illite-containing sediments, its ubiquitous presence in clay-rich clastic sediments is consistent with the relative rates of reaction as observed.

In summary, the observations of this study emphasize the significance of factors other than temperature—factors such as organic acids, permeability and pore fluid compositions—in affecting the rate and degree (and perhaps mechanism) of transformation of smectite to illite. These results are consistent with metastability of smectite and illite, wherein relative rates of reaction are determined by several interacting variables rather than by temperature alone.

## ACKNOWLEDGMENTS

This work was supported by NSF grant EAR-91-04565 to D. R. Peacor. The contribution by D. S. Coombs to this study was supported by the New Zealand Foundation for Research, Science and Technology. We are grateful to Dr. Y. Kawachi for electron microprobe analytical data. We also acknowledge Drs. E. J. Essene, I. MacKinnon and an anonymous reviewer for reviews. The STEM used in this study was acquired under NSF Grant no. EAR-87-08276, and the SEM under NSF Grant no. BSR-83-14092. This paper is Contribution No. 504 from the Mineralogical Laboratory, Department of Geological Sciences, University of Michigan.

## REFERENCES

Ahn JH, Peacor DR. 1986. Transmission and analytical electron microscopy of the smectite-to-illite transition. Clays Clay Miner 34:165–179.

Ahn JH, Peacor DR. 1987. Kaolinitization of biotite: TEM data and implications for an alteration mechanism. Am Mineral 72:353–356.

Ahn JH, Peacor DR. 1989. Illite/smectite from Gulf Coast shales: A reappraisal of transmission electron microscope images. Clays Clay Miner 37:542–546.

Ahn JH, Peacor DR, Coombs DS. 1988. Formation mechanisms of illite, chlorite and mixed layer illite-chlorite in Triassic volcanogenic sediments from the Southland Syncline, New Zealand. Contrib Mineral Petrol 99:82–89.

Boles JR. 1971. Synthesis of analcime from natural heulandite and clinoptilolite. Am Mineral 56:1724–1734.

Boles JR, Coombs. DS 1975. Mineral reactions in zeolitic Triassic tuff, Hokonui Hills, New Zealand. Geol Soc Am Bull 86:163–173.

Boles JR, Coombs. DS 1977. Zeolite facies alteration of sandstones in the Southland Syncline, New Zealand. Am J Sci 277:982–1012.

Boles JR, Franks SG. 1979. Clay diagenesis in Wilcox sandstones of southwest Texas: Implications of smectite diagenesis on sandstone cementation. J Sed Petrol 49:55–70.

Buatier M, Peacor DR, O'Neil JR. 1992. Smectite-illite transition in Barbados accretionary wedge sediments: TEM and AEM evidence for dissolution/crystallization at low temperature. Clays Clay Miner 40:65–80.

Burst JF. 1969. Diagenesis of Gulf Coast clayey sediments and its possible relation to petroleum migration. Am Assoc Petrol Geol Bull 53:73–93.

Cliff G, Lorimer GW. 1975. The quantitative analysis of thin specimens. J Microscopy 103:203–207.

Coombs DS. 1965. Sedimentary analcime rocks and sodium-rich gneisses. Mineral Mag 34:144–158.

Coombs DS. 1993. Dehydration veins in diagenetic zone and their significance to mineral facies. J Metam Geol 11:389–399.

Coombs DS, Cox S. 1991. Low and very low-grade metamorphism in southern New Zealand. Geol Soc New Zealand Misc Publ 58. 78 p.

Coombs DS, Ellis AJ, Fyfe WS, Taylor AM. 1959. The zeolite facies, with comments on the interpretation of hydrothermal syntheses. Geochim Cosmochim Acta 17:53–107.

Eberl DD. 1993. Three zones for illite formation during burial diagenesis and metamorphism. Clays Clay Miner 41:26–37.

Eggleton RA, Keller J. 1982. The palagonitization of limburgite glass—A TEM study. N Jb Miner Mh H7:321–336.

Essene EJ, Peacor DR. 1995. Clay mineral thermometry: A critical perspective. Clays Clay Miner 43:540–553.

Freed RL, Peacor DR. 1989. Variability in temperature of the smectite/illite reaction on Gulf Coast sediments. Clay Miner 24:171–180.

Freed RL, Peacor DR. 1992. Diagenesis and the formation of authigenic illite-rich I/S crystals in Gulf Coast shales: TEM study of clay separates. J Sed Petrol 62:220–234.

Grubb SMB, Peacor DR, Jiang W-T. 1991. Transmission electron microscopy observations of illite polytypism. Clays Clay Miner 39:540–550.

Hillier S, Matyas J, Matter A, Vasseur G. 1995. Illite/smectite diagenesis and its variable correlation with vitrinite reflectance in the Pannonian Basin. Clays Clay Miner 43: 174–183.

Hoffman J, Hower J. 1979. Clay mineral assemblages as low grade metamorphic geothermometers: Application to the thrust faulted disturbed belt of Montana. In: Scholle PA, Schluger PS, editors. Aspects of diagenesis. SEPM Spec Publ 26:55–79.

Hover VC, Walter LM, Peacor DR, Martini AM. 1995. K-uptake by smectite during early marine diagenesis in brackish and hypersaline depositional environments [abstract]. 32nd Clay Miner Soc Annual Meeting Program and Abstracts. p 61.

Hower J, Eslinger EV, Hower ME, Perry EA. 1976. Mechanism of burial metamorphism of argillaceous sediments: 1. Mineralogical and chemical evidence. Bull Geol Sci Am 87:725–737.

Huang W-L, Longo JM, Pevear DR. 1993. An experimentally derived kinetic model for smectite-to-illite conversion and its use as a geothermometer. Clays Clay Miner 41:162–177.

Inoue A, Kohyama N, Kitagawa R, Watanabe T. 1987. Chemical and morphological evidence for the conversion of smectite to illite. Clays Clay Miner 35:111–120.

Inoue A, Watanabe T, Kohyama N, Brusewitz AM. 1990. Characterization of illitization of smectite in bentonite beds at Kinekulle, Sweden. Clays Clay Miner 38:241–249.

Jiang W-T, Essene EJ, Peacor DR. 1990. Transmission electron microscopic study of coexisting pyrophyllite and muscovite: Direct evidence for the metastability of illite. Clays Clay Miner 38:225–240.

Jiang W-T, Peacor DR, Merriman RJ, Roberts B. 1990. Transmission and analytical electron microscopic study of mixed-layer illite/smectite formed as an apparent replacement of product of diagenetic illite. Clays Clay Miner 38: 449–468.

Jiang W-T, Nieto F, Peacor DR. 1992. Composition of diagenetic illite as defined by analytical electron microscope analyses: Implications for smectite-illite-muscovite transition [abstract]. 29th IGC Meeting Program and Abstracts; Kyoto, Japan. p 100.

Kawano M, Tomita K. 1992. Formation of allophane and beidellite during hydrothermal alteration of volcanic glass below 200°C. Clays Clay Miner 40:666–674.

Kim J-W, Peacor DR, Tessier D, Elsass F. 1995. A technique for maintaining texture and permanent expansion of smec-

tite interlayers for TEM observations. Clays Clay Miner 43:51–57.

Lahann RW. 1980. Smectite diagenesis and sandstone cement: the effect of reaction temperature. J Sed Petrol 50: 755–760.

Li G, Mauk JL, Peacor DR. 1995. Preservation of clay minerals in the Precambrian (1.1 Ga) Nonesuch Formation in the vicinity of the White Pine copper mine, Michigan. Clays Clay Miner 43:361–376.

Masuda H, Tanaka H, Gamo T, O'Neil JR, Peacor DR, Jiang W-T. 1992. Formation of authigenic smectite and zeolite and associated major element behavior during early diagenesis of volcanic ash in the Nankai Trough, Japan, ODP leg 131. In: Proc 7th International Symposium on Water-Rock Interaction. Rotterdam: Balkema. p 1659–1662.

Masuda H, O'Neil JR, Jiang W-T, Peacor DR. 1996. Relation between interlayer composition of authigenic smectite, mineral assemblages, I/S reaction rate and fluid composition in silicic ash of the Nankai Trough. Clays Clay Miner 44:443–459.

Nadeau PH, Wilson MJ, McHardy WJ, Tait JM. 1985. The conversion of smectite to illite during diagenesis: Evidence from some illite clays from bentonite and sandstones. Mineral Mag 49:393–400.

Perry EA, Hower J. 1970. Burial diagenesis in Gulf Coast pelitic sediments. Clays Clay Miner 29:165–177.

Perry EA, Hower J. 1972. Later-stage dehydration in deeply buried pelitic sediments. Am Assoc Petrol Geol Bull 56: 2013–2021.

Pollastro RM. 1989. Clay minerals as geothermometers and indicators of thermal maturity—Application to basin history and hydrocarbon generation. Am Assoc Petrol Geol Bull 73:1171.

Pollastro RM. 1990. The illite/smectite geothermometry—Concepts, methodology, and application to basin history and hydrocarbon generation. In: Nuccio VF, Barker CE, editors. Applications of thermal maturity studies to energy exploration, Rocky Mountain Section. Tulsa: SEPM. p 1–18.

Pollastro RM. 1993. Considerations and applications of the illite/smectite geothermometer in hydrocarbon-bearing rocks of Miocene to Mississippian age. Clays Clay Miner 41:119–133.

Powers MC. 1959. Adjustment of clays to chemical changes and the concept of the equivalent level. Clays Clay Miner 6:309–326.

Powers MC. 1967. Fluid release mechanisms in compacting marine mudrocks and their importance in oil exploration. Am Assoc Petrol Geol Bull 51:1240–1254.

Price KL, McDowell SD. 1993. Illite/smectite geothermometry of the Proterozoic Oronto Group, Midcontinent Rift System. Clays Clay Miner 41:134–147.

Pytte AM, Reynolds RC Jr. 1989. The thermal transformation of smectite to illite. In: Naeser ND, McColloh TH, editors. Thermal history of sedimentary basins. New York: Springer-Verlag. p 133–140.

Ramseyer K, Boles RJ. 1986. Mixed-layer illite/smectite minerals in Tertiary sandstones and shales, San Joaquin Basin, California. Clays Clay Miner 34:115–124.

Shau Y-H, Peacor DR. 1992. Phyllosilicates in hydrothermally altered basalts from DSDP Hole 504B, Leg 83—A TEM and AEM study. Contrib Mineral Petrol 112:119–133.

Small JS. 1994. Fluid composition, mineralogy and morphological changes associated with the smectite-to-illite reaction: an experimental investigation of the effect of organic acid anions. Clay Miner 29:539–554.

Small JS, Manning DAC. 1993. Laboratory reproduction of morphological variation in petroleum reservoir clays: Monitoring of fluid composition during illite precipitation. In: Manning DAC, Hall PL, Hughes CR, editors. Geochemistry of clay pore fluid interactions. London: Mineral Soc/ Chapman and Hall. p 181–212.

Środoń J, Eberl DD. 1984. Illite. In: Bailey SW, editor. Micas. Mineral Soc Am, Rev Mineral 13. p 495–544.

Sucha V, Kraus I, Gerthofferova H, Petes J, Serekova M. 1993. Smectite to illite conversion in bentonites and shales of the East Slovak Basin. Clay Miner 28:243–253.

Tazaki K, Fyfe WS, van der Gaast SJ. 1989. Growth of clay minerals in natural and synthetic glasses. Clays Clay Miner 37:348–354.

Tribble JS, Wilkens RH. 1994. Microfabric of altered ash layers, ODP leg 131, Nankai Trough. Clays Clay Miner 42: 428–436.

Veblen DR. 1992. Electron microscopy applied to nonstoichiometry, polysomatism, and replacement reactions in minerals. In: Buseck PR, editor. Minerals and reactions at the atomic scale: Transmission electron microscopy. Mineral Soc Am, Rev Mineral 27:181–229.

Velde B, Suzuki T, Nicot E. 1986. Pressure-temperature-composition of illite/smectite mixed-layer minerals: Niger Delta mudstones and other examples. Clays Clay Miner 34: 435–441.

Velde B. 1995. Comparative reaction rates of smectite to illite conversion in shales and volcanic ash layers [abstract]. 32nd Clay Miner Soc Annual Meeting Program and Abstracts. p 123.

Watanabe T. 1981. Identification of illite/montomorillonite interstratification by X-ray powder diffraction. J Miner Soc Jpn, Spec Issue 15:32–41.

Whitney G. 1990. Role of water in the smectite to illite reaction. Clays Clay Miner 38:343–350.

Yau Y-C, Peacor DR, McDowell SD. 1987. Smectite to illite reaction in Salton Sea shales: A transmission and analytical electron microscopy study. J Sed Petrol 57:335–342.

*(Received 18 January 1996; accepted 6 April 1996; Ms. 2730)*